On-Chip Sensor Substrate Requirements for Accurate Junction Temperature Measurements

Nick Baker[1], Nathan Carlson[1], Andrew Lemmon[1]

[1] University of Alabama, USA

Corresponding author: Nick Baker, nbaker2@ua.edu
Speaker: Nathan Carlson, ncarlson@crimson.ua.edu

Abstract

On-chip sensors are a promising way to monitor the junction temperature of power semiconductors. However, the sensor material, dimensions, and location, can impact the measured temperature. This paper assesses the accuracy and time response of an on-chip sensor according to its substrate thermal conductivity. Results are presented from Finite Element Simulations. It is found that for steady-state temperature measurements, the thermal conductivity of the substrate does not significantly impact the measured temperature. For example, from 10 W/mK to 200 W/mK substrate thermal conductivity, the temperature on the sensor surface remains within 0.01°C. On the other hand, for transient measurements at frequencies as low as 1 Hz, the impact of the sensor thermal conductivity is apparent.

1 Introduction

1.1 On-Chip Temperature Sensors

Many options exist for implementing on-chip junction temperature (T_J) sensors in power semiconductors. These range from integrated temperature sensing diodes [1][2], optical fibres [3][4], FBG sensors [5][6], and electrical sensors such as RTDs and thermistors [7]-[9]. In some cases, temperature sensors may be implemented underneath the chip in the DBC layer [10]. Each option may have distinct advantages and disadvantages. For example, optical fibres and FBG sensors are immune to EMI effects, however their mechanical placement can be challenging [3][6].

A common issue for all sensor types is ensuring a good thermal contact to the chip surface. For some optical fibre designs, the dielectric gel can reduce the quality of the contact to the chip [4]. FBG sensors are sensitive to strain, and therefore measurements may be impacted by the shore hardness and glass transition temperature of the adhesive used to attach the FBG to the chip [6]. In addition, expansion of the semiconductor chip during operation could also impact measurement results.

In the case of electrical sensors, Fig. 1 displays IR images of a Silicon IGBT during the final 1-millisecond of a 3-second 80 A current pulse. Fig. 1a shows an RTD on an Aluminium Nitride substrate with dimensions of 750 µm x 750 µm x 250 µm, while Fig. 1b shows an NTC thermistor with dimensions of 1 mm x 1 mm x 0.5 mm. The thermistor is based on a Vishay NTCC100E4 [11]. It is observed that the temperature of the top surface of each sensor is vastly different in each image.

Furthermore, video recordings of the heating and cooling of these devices over the 3-second heating and cooling period provide a visual demonstration of the difference in transient response of each sensor [12][13].

The general structure of a temperature sensor is shown in Fig. 2, where the temperature sensitive element of a sensor is deposited on the surface of a substrate material. As a result, the temperature dependent element is typically not in direct contact with the point of interest. For example, an FBG sensor may be constructed with a 100 µm – 150 µm coating of Polyimide [5], while RTDs or Thermistors may be constructed on a substrate of Aluminium Oxide [10][11], with thicknesses in the range of 150 µm [10] up to 550 µm [11]. Therefore, heat must travel through this material (or adhesive layer, if used) before a temperature can be measured. This can impact the accuracy and time response of the temperature sensor.

Thinner substrates or high conductivity materials, such as Aluminium Nitride, can improve the sensor performance, but may significantly increase man-

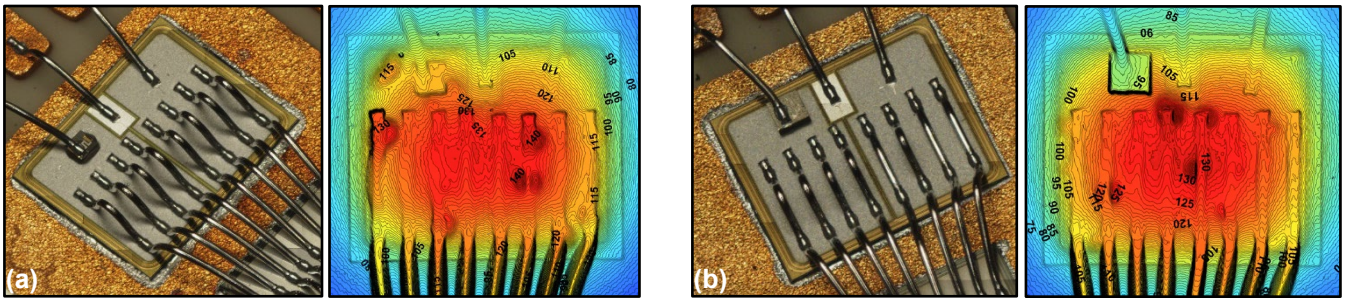

Fig. 1. (a) On-Chip Aluminium Nitride RTD sensor, (b) On-Chip NTC thermistor

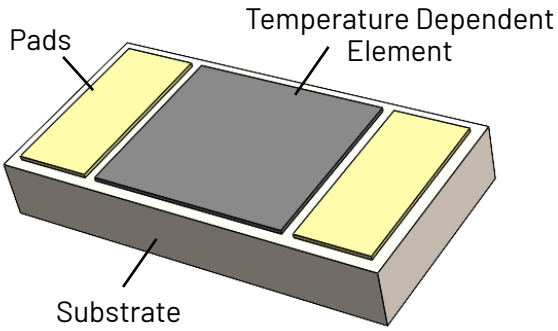

Fig. 2. General construction of an on-chip sensor (based on a Semitec FT Thermistor [12]).

ufacturing costs. This paper, therefore, investigates the impact of varying substrate thermal conductivity on the T_J measurement accuracy and time response of on-chip sensors.

The motivation for this work stems from prior experimental results, shown in Fig. 1. However, this paper primarily focuses on Finite Element simulations in COMSOL. Moreover, only the response of the material is the sensor material is considered – and not the response or bandwidth of the measurement unit used to interpret temperature data.

2 COMSOL Simulation

2.1 Electro-Thermal Study Setup

This study was conducted on a Wolfspeed CPM3-1700-R020E SiC MOSFET chip. The chip was modelled with 1-dimensional electrical conductivity in the active area regions. The active areas were coated with 4 µm of Aluminium metal to emulate the vertical conduction of individual MOSFET cells which are connected in parallel via the top and bottom metallization. We used 6 Aluminium wirebonds (300 µm diameter), a Silicon Nitride DBC with ceramic thickness of 0.25 mm, and a Copper baseplate of 3 mm. The mesh of the chip is shown in Fig. 3. Copper trace thicknesses on the DBC were 300 µm.

The Aluminium, Copper, and Solder materials (thickness of 50 µm for die attach, and 100 µm for DBC to baseplate) were modelled with a linearized temperature dependent resistivity. Furthermore, Silicon Carbide and Silicon Nitride were additionally modelled with a temperature dependent thermal conductivity. For example, Silicon Carbide is modelled with a thermal conductivity of 316 W/mK at 25°C, and 221 W/mK at 200°C. The properties of each material used in the simulation are summarized in Table 1.

Material	Electrical Conductivity (S / m)	Resistivity (Ω m)	Thermal Conductivity (W / mK)
Aluminium	-	$2.71\text{x}10^{-8}$ TCR: 0.0042	237
Copper	-	$1.72\text{x}10^{-8}$ TCR: 0.0039	404
SiC (Active Area)	472.4 205.1	-	316.5 232.5
SiC (Insulating)	-	$30\text{x}10^{30}$	316.5 232.5
Solder	-	$16.4\text{x}10^{-8}$ TCR: 0.004	57
Silicon Nitride	-	$30\text{x}10^{30}$	92.5 77.5
Sensor Substrate	-	$30\text{x}10^{30}$	0.2 to 200
Sensor Adhesive	-	$30\text{x}10^{30}$	3

Table 1 Electrical and Thermal properties of materials used in COMSOL simulation at 25°C. Red text denotes value at 175°C.

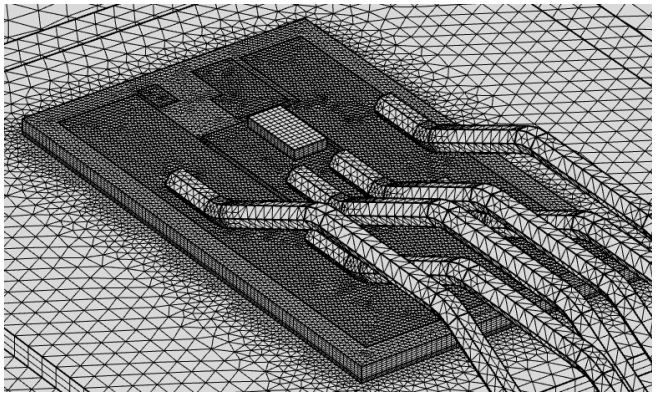

Fig. 3. Mesh from COMSOL for FE study

The bottom of the 3 mm Copper baseplate was assigned a heat-transfer coefficient of 7500 W/m^{2}K, while all other surfaces were assigned 20 W/m^{2}K to simulate natural convection to the ambient air.

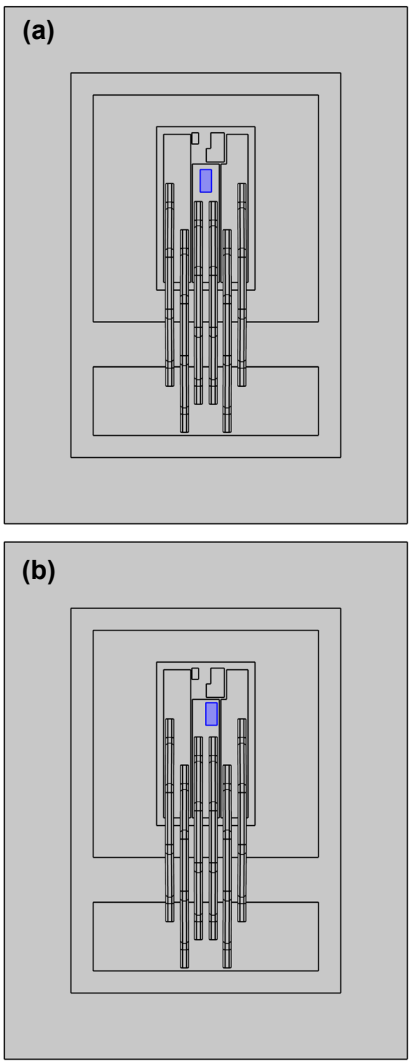

Fig. 4. Sensor locations.
(a) Central
(b) Off-Centre

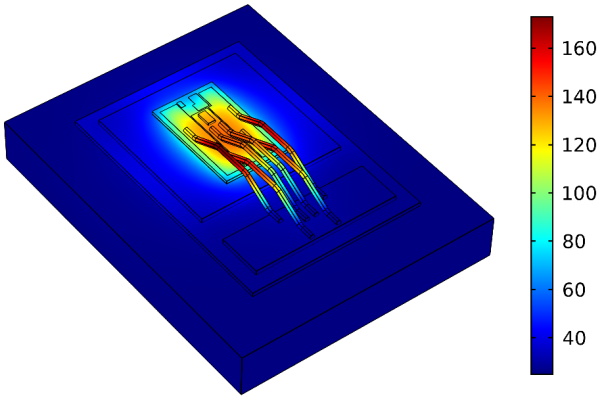

Fig. 5. Simulated temperature distribution across the chip during a joule-heating simulation.

The sensor was modelled with a geometry according to Fig. 2 – where the temperature dependent element is isolated from the chip via a substrate material. Therefore, the temperature measured by the sensor was estimated from the mean temperature of the top surface of the substrate. This region is highlighted in blue in Fig. 4.

The sensor's length and width were 1 mm x 0.5 mm. In Section 2.2 and 2.3, the substrate thickness was 150 µm. Additional thicknesses were also assessed in Section 2.4.

For R&D purposes, on-chip sensors are most commonly placed by hand. This gives rise to human error in sensor placement. Therefore, we simulated two sensor placements shown in Fig. 4. Both sensor locations avoid mounting across a gate finger, which can lead to a damaged chip [16][17]. The difference between the two positions in X-Y dimensions is 250 µm and 100 µm. Furthermore, the sensor adhesive is modelled as a 7.5 µm layer with a thermal conductivity of 3 W/mK.

The T_J of the chip was calculated as the mean temperature of the three active regions and surface metallization of the chip. Non-active areas of the chip were not included. Fig. 5 displays the simulated temperature distribution across the chip.

2.2 Steady-State Results

The simulation was performed using a heating current of 70.7 A, with the thermal conductivity of the sensor substrate swept logarithmically from 0.2 W/mK to 200 W/mK.

Results are shown in Fig. 6. The mean T_J was consistent at 123.1°C for all substrate conductivities. At 0.2 W/mK substrate thermal conductivity, the sensor temperature in position A was 126.8°C, while the sensor temperature at 200 W/mK increased to 129.1°C. However, it should be noted that the difference in sensor temperature from

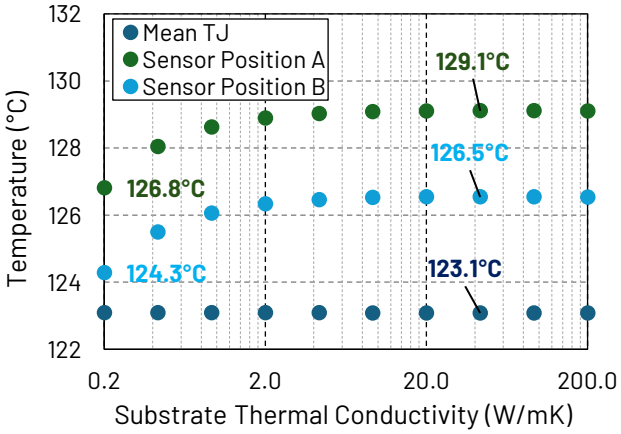

Fig. 6. COMSOL stationary study results at 70.7 A heating current vs. sensor substrate thermal conductivity.

2.0 W/mK to 200 W/mK is just 0.2°C, and from 10 W/mK the sensor temperature remains within 0.01°C.

These results appear to indicate that thermal conductivity materials as low as 10 W/mK (if the substrate thickness is 150 µm or less) are sufficient for on-chip temperature sensing in steady-state conditions.

However, a discrepancy in sensor temperature between position A and position B is evident. This is approximately 2.5°C at all simulated thermal conductivities. As identified in other studies using on-chip sensors [18]-[20], the accuracy of the sensor in comparison to the mean T_J is dependent on the sensor location due to the non-uniform temperature distribution across the chip. From Fig. 6, it could further be deduced that small discrepancies in sensor placement (within the range of human error), can have as much impact on temperature measurement accuracy as the design of the sensor itself.

Note that this study has not considered additional mounting errors such as non-uniform adhesive contact or a tilted sensor.

Since the measured temperature by the sensor is highly dependent on its location, Table 2 further displays the sensor temperature in Position A vs. the temperature of the Aluminium metallization on which the sensor is adhered to.

Thermal Conductivity (W / mK)	Sensor Bond Location (°C)	Sensor Temperature (°C)
0.2	129.14	126.81
0.4	129.14	128.04
0.9	129.14	128.62
2.0	129.14	128.89
4.3	129.14	129.02
9.3	129.14	129.08
20.0	129.13	129.10
43.1	129.13	129.11
92.8	129.12	129.11
200.0	129.12	129.10

Table 2 Sensor temperature vs. temperature of the Aluminium metallization at the sensor bond location in Position A.

2.3 Transient Results

The transient response was assessed from 1 Hz to 200 Hz. The specific heat capacity of the sensor was modelled as 900 J/kg°C with a density of 3900 kg/m^3. The 7.5 µm adhesive layer was modelled with 900 J/kg°C and 1500 kg/m^3. A 28 A peak-to-peak sinusoidal heating current was applied to the device, with a DC offset of 70 A. This corresponds to an RMS current of 70.7 A (which is the current used in Section 2.2). Therefore, the results of the steady-state study were used as the initial conditions for transient study.

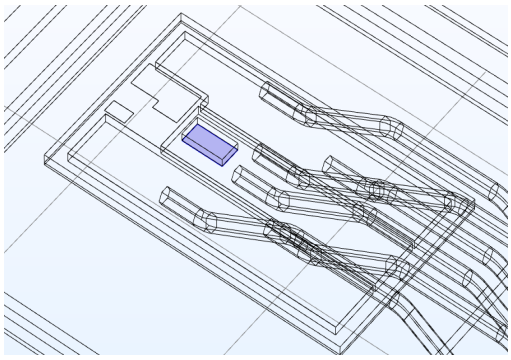

Fig. 7. Location on chip surface used for transient measurement comparisons.

The following results are compared to the chip temperature at the sensor bonding location in Position A, which is highlighted in Fig. 7.

2.3.1 Results at 1 Hz

Fig. 8 shows simulation results for 500-milliseconds at 1 Hz load frequency. The maximum time step was limited to 500 µs. Results from each substate thermal conductivity, as well as the sensor bond location are shown.

Below 1 W/mK, the sensor response is significantly attenuated. For example, at 0.43 W/mK, the peak sensor temperature is 160.9°C in comparison to 165.6°C. At 0.2 W/mK, this discrepancy is over 10°C. From 9.3 W/mK to 200 W/mK, however, sensor temperatures are within 0.2°C of the bond location at all time points.

2.3.2 Results at 200 Hz

Fig. 9 shows simulation results from 60- to 80-milliseconds at 200 Hz load frequency. In this simulation, the maximum time step was limited to 80 µs.

It can be observed that no substrate thermal conductivity allows the temperature swing at 200 Hz to be tracked. At 200 W/mK and 92.8 W/mK, the sensor temperature experiences a swing of approximately 3°C peak-to-peak. However, the temperature of the chip surface at the sensor location has a swing of just over 5°C.

At substrate thermal conductivities below 1 W/mK, it can be further observed that there is a sensor temperature offset. For example, at 0.2 W/mK, the sensor temperature is within ± 0.15°C around 127°C at all time points. This is at the bottom of the peak-to-peak swing seen by the chip at the sensor location. Therefore, the maximum temperature experienced by the chip in the sensor location is underestimated by approximately 5°C.

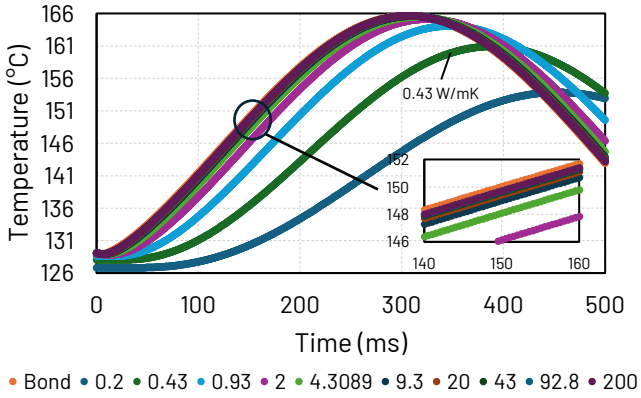

Fig. 8. Sensor temperature vs. substrate thermal conductivity at 1 Hz load frequency.

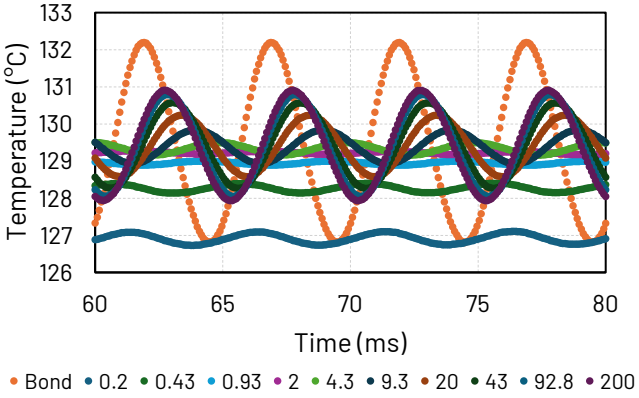

Fig. 9. Sensor temperature vs. substrate thermal conductivity at 200 Hz load frequency.

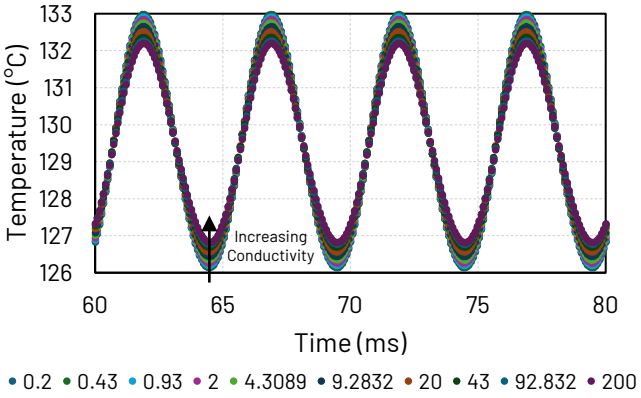

Fig. 10. Temperature of Aluminium metallization at the sensor position vs. sensor substrate thermal conductivity at 200 Hz load frequency.

Additionally, Fig. 10 shows that there is a localized impact on the chip surface temperature as the sensor thermal conductivity is varied. It is noted that the temperature swing increases approximately 1.7°C from the highest to lowest simulated thermal conductivity (200 W/mK to 0.2 W/mK). It is assumed that the low conductivity substrates hinder heat transfer to the ambient. Nevertheless, the overall impact on the mean T_J was negligible.

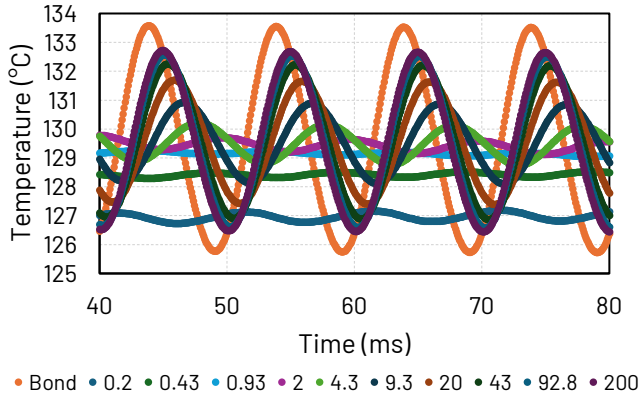

Fig. 11. Temperature of Aluminium metallization at the sensor position vs. sensor substrate thermal conductivity at 100 Hz load frequency.

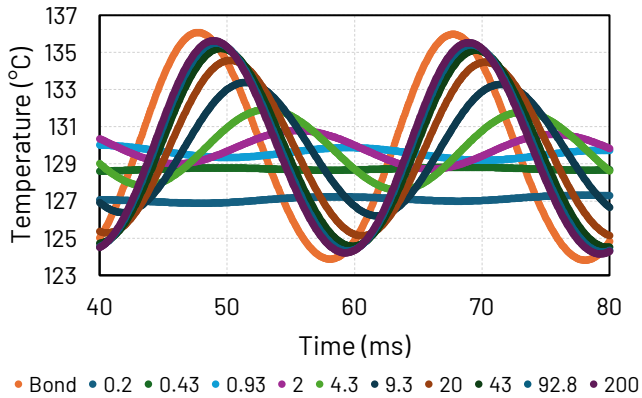

Fig. 12. Temperature of Aluminium metallization at the sensor position vs. sensor substrate thermal conductivity at 50 Hz load frequency.

2.3.3 Results at 100 Hz

Fig. 11 displays simulation results from 40- to 80-milliseconds at 100 Hz load frequency. Similar trends to the 200 Hz condition are apparent. No thermal conductivity allows tracking of the full temperature swing at the sensor location. Furthermore, low conductivities also show an offset in temperature measurement. This offset becomes negligible above 2.0 W/mK, where the measured temperature is aligned with the mid-point of the sinusoidal temperature evolution. This is consistent with steady-state simulation results shown in Table 2.

2.3.4 Results at 50 Hz

Load frequencies of 50 Hz and 60 Hz may be of interest since these are the most common frequencies used in grid applications. Therefore, Fig. 12 shows simulation results at this frequency. The benefits beyond 43 W/mK thermal conductivity appear to be minimal.

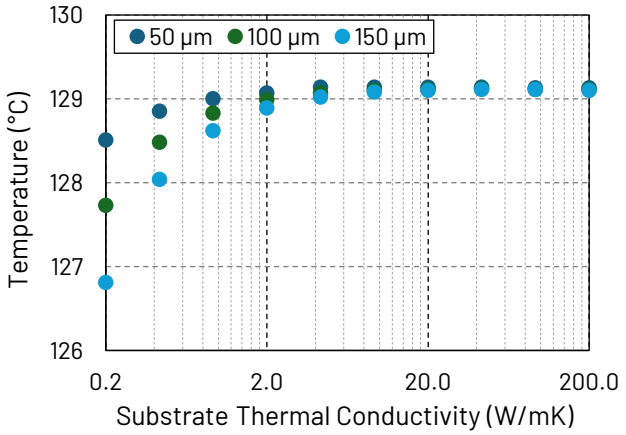

Fig. 13. COMSOL stationary study results at 70.7 A heating current vs. sensor substrate thermal conductivity at varying substrate thickness.

2.4 Impact of Sensor Thickness and Material

Thus far, simulations have been performed with a logarithmic sweep of thermal conductivity on a fixed thickness substrate of 150 µm. The highest simulated conductivity, 200 W/mK, is beyond the thermal conductivity of high-performance materials such as Aluminium Nitride. In addition, manufacturing sensors at this thickness with this material may be challenging.

Therefore, this section simulates the sensor response using an Alumina substrate of 100 µm thickness, and a Glass substrate of 50 µm thickness. These substrate materials and dimensions appear to be readily available [12]. Alumina was modelled with a thermal conductivity of 33 W/mK, while Glass was modelled with 1.5 W/mK. In both cases, the heat capacity was still modelled again as 900 J/kg°C. However, for the Glass substrate, the density was lowered to 2200 kg/m^3.

2.4.1 Steady-State

Fig. 13 shows the impact of varying substrate thicknesses for steady-state measurements. The test conditions are identical to Fig. 6. While the offset at low thermal conductivities is reduced with a thinner 50 µm substrate, it still appears that conductivities above 2 W/mK are required for accurate steady-state measurements.

2.4.2 Transient Response at 50 Hz and 100 Hz

Fig. 14 and 15 display the response at 50 Hz and 100 Hz respectively. For 100 Hz, the 100 µm Alumina and 50 µm Glass substrate underestimate the temperature swing by just under 2°C. However, for 50 Hz, these substrates closely track the swing and underestimate by just 0.5°C.

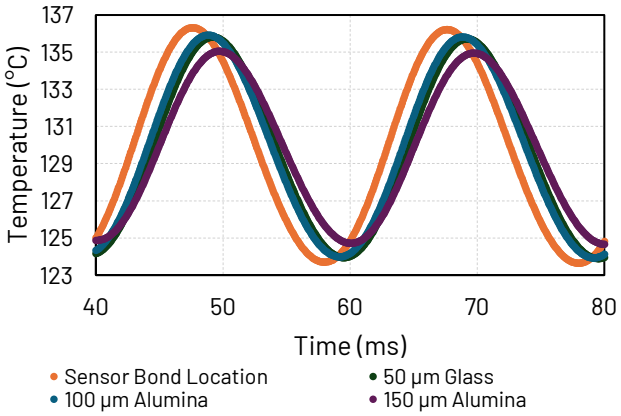

Fig. 14. Temperature of Aluminium metallization at the sensor position vs. sensor substrate thermal conductivity at 50 Hz load frequency.

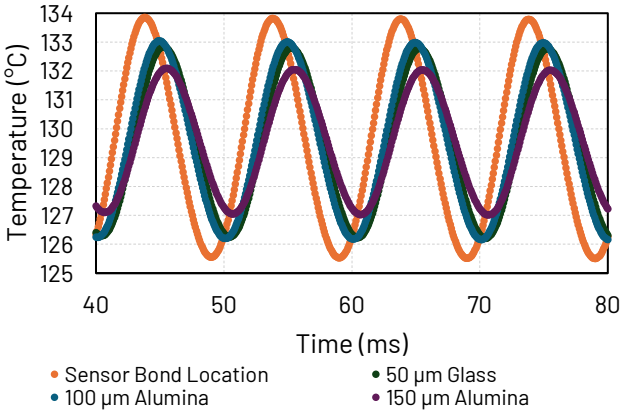

Fig. 15. Simulated temperatures of Alumina and Glass sensor with differing substrate thickness at 100 Hz.

The response of the on-chip sensors could further be improved by using 30 µm substrates or thinner, higher performance materials, or different sensor designs (such as flip-chip, where the temperature sensitive element is directly contacted to the chip). However, the cost and complexity of handling and mounting the sensor is likely to increase. In addition, for general development work (such as validating cooling designs or thermal models), steady-state and measurements up to 50 Hz may be sufficient. Furthermore, given the results in Section 2.2, reliable and repeatable temperature measurements are perhaps more dependent on the sensor mounting process than on the design of the sensor.

3 Conclusion

This paper used Finite Element simulations to assess the measurement accuracy and transient response of on-chip junction temperature sensors with varying substrate thermal conductivity. It was found that for sensors with a substrate thickness of 150 µm and below, substrates 10 W/mK and

above are sufficient for steady-state measurements. In fact, the use of substrates from 0.2 W/mK to 200 W/mK altered the sensor temperature by just 2.3°C in comparison to a mean junction temperature of 123.1°C. The sensor placement, however, was found to impact the measured temperature by 2.6°C with only a 200 µm x 100 µm displacement.

For transient performance, no simulated substrate thermal conductivity allowed tracking of junction temperature swings at frequencies of 100 Hz and 200 Hz. At 50 Hz, a thermal conductivity above 40 W/mK appeared to provide minimal benefits on a 150 µm substrate. However, thinner substrates of 100 µm Alumina and 50 µm Glass appeared to be sufficient in tracking temperature swings at 50 Hz. This performance may be sufficient for most development applications, and it may be worth considering whether higher performance materials or sensor designs are necessary for junction temperature measurement in power electronic converters.

4 Acknowledgements

This research was funded by the United States Office of Naval Research, under grant number N000142412508.

Approved, DCN# 2025-2-22-648.

DISTRIBUTION STATEMENT A. Approved for public release: distribution is unlimited.

References

[1] E.R. Motto, J.F. Donlon, “IGBT Module with User Accessible On-Chip Current and Temperature Sensors”, in Applied Power Electronics Conference and Exposition (APEC), pp. 176-181, Orlando, Florida, Feb. 5-9, 2012.

[2] Infineon Application Note AN111546, “600 V CoolMOS™ S7 with temperature sense”, July 2024.

[3] M. Piton, B. Chauchat, J.F. Servière, “Implementation of direct Chip junction temperature measurement in high power IGBT module in operation – Railway traction converter,” Microelectronics Reliability, Volumes 88–90, 2018, Pages 1305-1310.

[4] K. Zhang, C. Leduc and F. Iannuzzo, "Comparison of Junction Temperature Measurement Using the TSEP Method and Optical Fiber Method in IGBT Power Modules without Silicone Gel Removal," PCIM Europe 2023; International Exhibition and Conference for Power Electronics, Intelligent Motion, Renewable Energy and Energy Management, Nuremberg, Germany, 2023, pp. 1-8.

[5] S. Chen, D. Vilchis-Rodriguez, M. Barnes and S. Djurović, "A Comparison of Chip Temperature Acquisition Technologies of IGBT Power Modules," in IEEE Sensors Journal, vol. 24, no. 12, pp. 19107-19116, 15 June15, 2024, doi: 10.1109/JSEN.2024.3390600.

[6] S. Chen, D. Vilchis-Rodriguez, M. Barnes and S. Djurović, "Direct On-Chip IGBT Thermal Sensing Using Adhesive Bonded FBG Sensors," in IEEE Sensors Journal, vol. 23, no. 19, pp. 22507-22516, 1 Oct.1, 2023, doi: 10.1109/JSEN.2023.3301070.

[7] N. Baker, L. Dupont, S. M. Beczkowski and F. Iannuzzo, "Proof-of-Concept for an On-Chip Kelvin-Emitter RTD Sensor for Junction Temperature Monitoring of IGBTs," in IEEE Transactions on Components, Packaging and Manufacturing Technology, doi: 10.1109/TCPMT.2024.3370951.

[8] N. Baker, F. Iannuzzo, S. Beczkowski and P. K. Kristensen, "Proof-of-Concept for a Kelvin-Emitter On-Chip Temperature Sensor for Power Semiconductors," 2019 21st European Conference on Power Electronics and Applications (EPE '19 ECCE Europe), Genova, Italy, 2019, pp. P.1-P.8, doi: 10.23919/EPE.2019.8914963.

[9] S. Fröhling, D. Herwig and A. Mertens, "Contact-integrated temperature measurement for power modules," 2021 23rd European Conference on Power Electronics and Applications (EPE'21 ECCE Europe), Ghent, Belgium, 2021, pp. P.1-P.11.

[10] R. Ke, Z. Hu, J. Tao, Z. Yang and C. Liu, "A Novel Method for Online Junction Temperature Monitoring of Power Module Based on In-Situ Sensor Fabrication," in IEEE Transactions on Power Electronics, vol. 40, no. 2, pp. 3518-3529, Feb. 2025, doi: 10.1109/TPEL.2024.3485997.

[11] https://www.vishay.com/docs/29058/ntcc100e.pdf [accessed 6th October 2024].

[12] https://www.semitec-global.com/products/thermistor_ft/ [accessed 8th October 2024].

[13] https://yageo-nexensos.com/content/dam/nexensos/documents/whitepaper/Whitepaper_SMD-SC_EN.pdf [accessed 8th October 2024].

[14] https://www.youtube.com/watch?v=4F7DE9YULYE [accessed 15th February 2025].

[15] https://www.youtube.com/watch?v=rCJykoleaDw [accessed 15th February 2025].

[16] N. Baker, F. Iannuzzo, S. Bęczkowski, “Multi-Chip Temperature Imbalance of SiC MOSFETs in MOSFET vs. Body-Diode Conduction,” 8th – 10th April 2025, 2025 IEEE International Workshop on Integrated Power Packaging (IWIPP), Tuscaloosa, Alabama, USA.

[17] Baker, Nick, Impact of Operating Mode on Chip Temperature Imbalance in Multi-Chip Sic Mosfet Power Modules. Available at SSRN: https://ssrn.com/abstract=5146705 or http://dx.doi.org/10.2139/ssrn.5146705

[18] N. Baker, L. Dupont, S. Munk-Nielsen, F. Iannuzzo and M. Liserre, "IR Camera Validation of IGBT Junction Temperature Measurement via Peak Gate Current," in IEEE Transactions on Power Electronics, vol. 32, no. 4, pp. 3099-3111, April 2017, doi: 10.1109/TPEL.2016.2573761.

[19] J. Brandelero, J. Ewanchuk and S. Mollov, "Selective Gate Driving in Intelligent Power Modules," in *IEEE Transactions on Power Electronics*, vol. 36, no. 1, pp. 898-910, Jan. 2021, doi: 10.1109/TPEL.2020.3002188.

[20] M. Denk and M. -M. Bakran, "Comparison of UCE- and RGi-based junction temperature measurement of multichip IGBT power modules," *2015 17th European Conference on Power Electronics and Applications (EPE'15 ECCE-Europe)*, Geneva, Switzerland, 2015, pp. 1-11, doi: 10.1109/EPE.2015.7309067.